THE ASTRONOMICAL JOURNAL, 121:2761–2768, 2001 May
© 2001. The American Astronomical Society. All rights reserved. Printed in U.S.A.

X-RAY AND OPTICAL SPECTRA OF THE UNUSUAL CATACLYSMIC VARIABLES LS PEGASI AND T LEONIS

PAULA SZKODY[1] AND KAORI NISHIKIDA
Department of Astronomy, University of Washington, Box 351580, Seattle, WA 98195; szkody@astro.washington.edu, kaori@astro.washington.edu
KNOX S. LONG
Space Telescope Science Institute, 3700 San Martin Drive, Baltimore, MD 21218; long@stsci.edu
AND
ROBERT FRIED
Braeside Observatory, P.O. Box 906, Flagstaff, AZ 86002; captain@braeside.org
Received 2000 October 13; accepted 2001 January 16

ABSTRACT

We obtained *ASCA* observations of the cataclysmic variables LS Peg and T Leo in order to refine the X-ray characteristics of these two systems with unusual stream behaviors and to search for orbital features that might signify the presence of material above the orbital plane. Simultaneous (LS Peg) and contemporaneous (T Leo) optical observations showed the systems undergoing their typical stream behaviors (absorption, high-velocity component, and quasi-periodic oscillations in LS Peg; stream flow to the far side of the disk in T Leo). The X-ray light curve of LS Peg shows a low but constant count rate throughout its orbit. To fit the spectrum with a reasonable temperature requires a 7 keV partial-absorber model with high column (6×10^{22} cm^{-2}). This may be evidence for material thrown high above the disk by the disk-stream interaction or a magnetic accretion funnel sometimes suggested to explain other SW Sex stars. The spectrum of T Leo is consistent with a simple 4–6 keV thermal model with lower column ($3–5 \times 10^{20}$ cm^{-2}) and a small contribution from a cooler 1 keV component. Its light curve shows enhanced flux between phases 0.8 and 1.0, which is not due to a change in temperature or column. The difference in behavior of this light curve from that of U Gem may be due to the lower accretion in this shorter period system.

Key words: novae, cataclysmic variables — stars: individual (LS Pegasi, T Leonis) — X-rays

1. INTRODUCTION

Cataclysmic variables (CVs) undergo large changes in X-ray flux and spectra during their dwarf novae cycles (see summaries in Warner 1995; Verbunt et al. 1997). However, variability associated with their short (usually less than 2 hr) orbital periods is not so apparent except for systems at high inclination, in which eclipses may be observed. An exception is U Gem, which was found to have periodic orbital dips at outburst (Mason et al. 1988; Long et al. 1996), and these dips were found to persist at quiescence (Szkody et al. 1996). These latter observations showed that *ASCA* is a good probe of absorbing material above the plane, since to have dips visible at the 65° inclination of U Gem the material must be located far from the orbital plane.

The *ASCA* spectra of U Gem could be fitted with a single-temperature component of about 7 keV and increased system absorption near phase 0.7. The energy and phase dependence of these dips are reminiscent of those seen in some low-mass X-ray binaries. Frank, King, & Lasota (1987) explain these dips as the interaction of the accretion stream with the disk, which splashes material out of the plane to form cool clouds that obscure the radiation produced close to the white dwarf. These ideas received support from the three-dimensional numerical calculations of Hirose, Osaki, & Mineshige (1991) and Armitage & Livio (1996, 1998), which showed that material can be thrown up to several scale heights. These models also showed that resonances in the disk can produce bulges at phases 0.2, 0.5, and 0.8. When viewed at the right angle, these bulges could also result in some absorption of X-rays. Magnetic CVs have also shown X-ray absorption dips when the stream flow to the accretion column occults the white dwarf's emitting area (Watson 1995).

Since observations of these dips can provide important constraints on the size and density of the stream region, we attempted to find further evidence for them in two bright known X-ray–emitting CVs with low inclinations and optical signatures of unusual stream flow. One is LS Peg (formerly known as S193), a $V = 12$th–14th magnitude CV with an orbital period of 4.2 hr and an inclination of 30°. It has recently been proposed as an SW Sex star (Szkody et al. 1997; Taylor, Thorstensen, & Patterson 1999, hereafter TTP; Martinez-Pais, Rodriguez-Gil, & Casares 1999, hereafter MRC), because it shows a large-amplitude (1700 km s^{-1}) component in its radial velocity curve, absorption in the Balmer and He I lines at some phases, and quasi-periodic oscillations in its light curve at a period close to 20 minutes. The other is the $V = 10$–15.5 mag ultrashort-period (85 minutes) system T Leo, for which spectroscopic observations indicate an inclination near 60° and a stream component located on the opposite side of the accretion disk from a normal stream impact point (Shafter & Szkody 1984, hereafter SS84). Our study of these two systems, reported below, included both X-ray observations throughout an orbit with *ASCA* and simultaneous or contemporaneous optical observations.

[1] Based on observations with the Apache Point Observatory (APO) 3.5 m telescope, which is owned and operated by the Astrophysical Research Consortium.

TABLE 1

SUMMARY OF OBSERVATIONS

UT	Observatory	UT Interval	Comments
LS Peg:			
1998 Nov 23	BO	01:06–05:59	*V* filter 30 s integrations
1998 Nov 24	BO	01:03–06:00	*V* filter 30 s integrations
1998 Nov 24	APO	02:01–05:44	36 *B*, *R* spectra 300s integrations
1998 Nov 23/24.....	*ASCA*	12:39–09:30	22 ks (SIS), 25 ks (GIS) good time
T Leo:			
1998 Dec 13.....	*ASCA*	01:20–21:15	26 ks (SIS), 30 ks (GIS) good time
1998 Dec 14.....	APO	10:10–13:11	22 *B*, *R* spectra 300 s integrations

2. OBSERVATIONS

The *ASCA* satellite observed LS Peg on 1998 November 23–24 and T Leo on 1998 December 14. *ASCA* uses four co-aligned telescopes with detectors that provide data in the 0.5–10 keV energy range (Tanaka, Inoue, & Holt 1994). We used the 1-CCD mode of the CCD detectors (SIS0 and SIS1). The other two detectors (GIS2 and GIS3) are xenon-filled gas scintillation proportional counters. Each detector has certain advantages; i.e., the SIS has better overall energy resolution and has more effective area below 1.5 keV, while the GIS has more sensitivity above 5 keV.

FTOOLS Version 4.2 was used for screening the data and extracting light curves and spectra. Low bit-rate data, times when the satellite was in the South Atlantic Anomaly (SAA), and time intervals with deviation of more than 0°.01 from the mean pointing were rejected. Other screening criteria common to both the SIS and GIS included the angular distance between the target and the Earth's limb (the elevation angle) and the cutoff rigidity. Data were rejected when the elevation angle was smaller than 10° (5°) or the cutoff rigidity was lower than 6 (4) GeV c^{-1} for the SIS (GIS). Additionally for the SIS, time intervals were excluded when the angle between the target and the bright Earth's limb was less than 20°, as well as the first 16 s following either a passage through the SAA or the day-night transition. Hot and flickering pixels were removed and only grade 0, 2, and 4 were used. For the GIS, the standard REV2 screening was applied, which excluded regions with high particle background and flares.

After screening, the net resulting good exposure times for LS Peg were 21,664 s (SIS) and 25,288 s (GIS) and for T Leo were 25,873 s (SIS) and 30,460 s (GIS). Source light curves and spectra were extracted from circular regions centered on the source with a radius of 3′ for LS Peg SIS (4′ radius for T Leo) and 5′ for the GIS. Background spectra for the SIS were extracted from the entire CCD excluding the source region, while for the GIS they were extracted from circular regions with 5′ radius near the center of the GIS field of view. The count rates and error bars were determined by inputting the data and background files into XSPEC and obtaining the background-subtracted rate for the observation.

Optical photometry and spectra were obtained during the *ASCA* observation of LS Peg, and spectra were obtained for T Leo 13 hours after the *ASCA* observation. The photometry was obtained at the Braeside Obseratory (BO) 0.4 m telescope using a CCD and a *V* filter, while the spectra were obtained with the Double Imaging Spectrograph (DIS) at the 3.5 m APO telescope. Blue and red spectra were obtained throughout the orbits of both systems, using a 1″.5 slit and covering 4200–5000 Å and 5800–6800 Å at about 2.5 Å resolution. The spectra were calibrated with lamps for wavelength and standards for flux using standard reduction routines within IRAF. A summary of all the observations is provided in Table 1. The optical observations showed that LS Peg was at its usual high state of 12th magnitude and T Leo was at its usual quiescent state of 15th during the X-ray observations.

3. LS PEG

The *ASCA* count rates for LS Peg (Table 2) were lower than expected based on previous *Ginga* data (Szkody et al. 1994). These *Ginga* observations in 1989 were consistent with a hard (15 keV) spectrum, while previous *ROSAT* observations in 1992 (also in Szkody et al. 1994) showed a softer (1 keV) component. Since the *Ginga* and *ROSAT* observations were separated by 3 years and LS Peg was at 13th magnitude during the *Ginga* observation and at 12th magnitude during the *ROSAT* one, it had not been clear whether the different spectra resulted from a change in the accretion rate or if there are typically two components in this object that were measured with the satellites best suited to hard (*Ginga*) and soft (*ROSAT*) energies. The reason for the count rate differences between *ASCA* and *Ginga* and the different components between *Ginga* and *ROSAT* became apparent with the *ASCA* GIS images, showing two sources that likely contributed to the *Ginga* flux. One source is LS Peg, and the other is an extended source located at 10′ west and 19′ south of LS Peg that is labeled as a cluster of galaxies in the pointed WGACAT catalog from Goddard.

The SIS0 and SIS1 spectra (and similarly the GIS2 and GIS3) of LS Peg were combined (using Gaussian errors), an average response matrix was created, and the combined spectra were regrouped so that each bin contained at least 25 counts. The background-subtracted count rates are low,

TABLE 2

COUNT RATES[a]

Detector	LS Peg	T Leo
SIS0	0.029 ± 0.002	0.325 ± 0.003
SIS1	0.023 ± 0.002	0.254 ± 0.003
SIS.....	0.026 ± 0.001	0.290 ± 0.002
GIS2.....	0.017 ± 0.001	0.162 ± 0.003
GIS3.....	0.026 ± 0.001	0.184 ± 0.003
GIS	0.020 ± 0.001	0.173 ± 0.002

[a] Count rate (in counts per second) is over energy range 0.6–8 keV for SIS and 0.8–8 keV for GIS; SIS and GIS are combined data for detectors of each type.

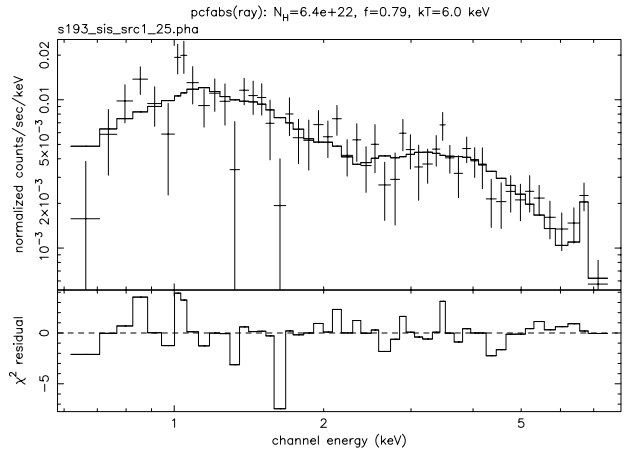


FIG. 1.—One-temperature plasma emission model fitted to the combined SIS spectrum of LS Peg.

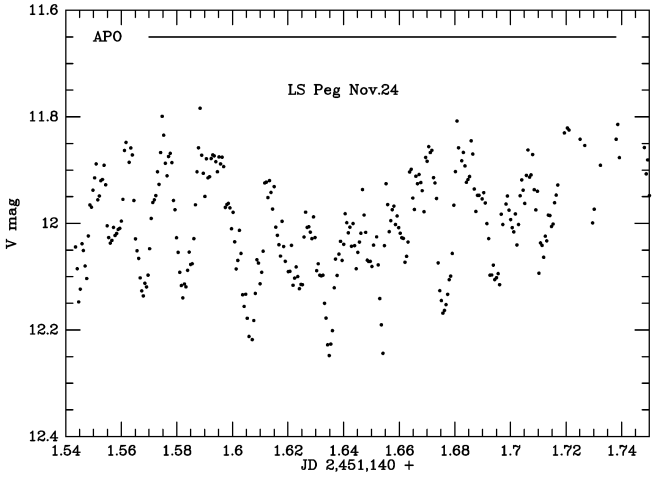


FIG. 2.—Optical light curve of LS Peg during the *ASCA* observations. Each point is a 30 s integration with error bar of 0.01 mag. The solid line is the time interval of the APO spectra.

0.026 ± 0.001 and 0.021 ± 0.001 counts s^{-1} for SIS and GIS, respectively (Table 2 gives individual rates for each detector). The spectra were fitted with a variety of models within XSPEC Version 10, including single-component thermal models (brem, raymond, and mekal) with column absorption, models with a partial covering absorber (pcf), and combinations of several components. Attempts to fit the spectra with any single- or multiple-component model with a uniform absorber did not fit the spectrum well (unrealistic temperatures greater than 65 keV were produced). But a partially absorbed model with a large column and covering fraction does fit the data (results and 90% confidence intervals are summarized in Table 3). We find that a one-temperature ($kT \sim 6$–7 keV) model gives an adequate fit to the data. The addition of a second component reduces the residuals below 1 keV, although the addition of the second component is not required statistically. For the single-component model, the 2–6 keV flux is 1.1×10^{-12} ergs s^{-1} cm^{-2}. Figure 1 shows this one-component fit to the combined SIS spectrum.

This type of model fit, along with the high column, is not unusual for magnetic cataclysmic variables (Ishida, Fujimoto, & Matsuzaki 1996) in which there is an accretion column. As some explanations of the peculiarities of the SW Sex stars have involved magnetic scenarios (Casares et al. 1996), this is an interesting coincidence. The recent discovery of circular polarization in LS Peg (Rodriguez-Gil et al. 2001) provides a strong argument for magnetic accretion in this system and for SW Sex stars in general. Alternatively, the high column could be a by-product of the impact scenarios predicted by Armitage & Livio (1998), which have been used to explain the phase-dependent absorption evident in the optical spectra of the SW Sex stars (Hoard, Thorstensen, & Szkody 2000). The large accretion rate in LS Peg may produce a halo of material above the disk, with the largest concentration at the stream impact point. The low inclination of the system means that this material is viewed throughout the orbit.

X-ray light curves in the energy ranges 0.6–8.0 keV and 0.8–8.0 keV were extracted from the SIS and GIS data, respectively, and were folded on the orbital period of 0.174774 days (TTP). The folded light curves do not show any significant variation throughout the orbit. The optical data obtained before and during the *ASCA* observation show the usual prominent flickering (Fig. 2 shows the data simultaneously with the X-ray and optical spectra). A Fourier transform of the photometric data shows enhanced power at the usual quasi-periodic timescale of 19 minutes (Garnavich & Szkody 1992; TTP), which is evident by eye

TABLE 3

XSPEC MODEL PARAMETERS FOR FITS TO LS PEG *ASCA* SPECTRA

	ABSORBER		HOT COMPONENT		COOL COMPONENT		
DETECTOR AND MODEL[a]	N_H[b]	f[c]	kT_1[d]	N_1[e]	kT_2[d]	N_2[e]	χ^2_ν
SIS:							
pcf(ray)	$6.4^{+2.9}_{-1.9}$	$0.79^{+0.07}_{-0.08}$	$6.0^{+4.2}_{-1.8}$	$1.9^{+0.7}_{-0.4}$	...	...	51/48 = 1.1
pcf(ray+ray)	$5.1^{+2.5}_{-1.5}$	$0.83^{+0.07}_{-0.09}$	$7.0^{+5.0}_{-2.6}$	$1.7^{+0.4}_{-0.3}$	$1.1^{+0.39}_{-0.30}$	$0.25^{+0.66}_{-0.23}$	47/47 = 1.0
GIS:							
pcf(ray)	$5.5^{+2.3}_{-1.8}$	$0.83^{+0.04}_{-0.08}$	$6.5^{+5.1}_{-2.7}$	$2.1^{+1.1}_{-0.4}$	...	...	59/64 = 0.94
pcf(ray+ray)	$4.4^{+2.4}_{-1.7}$	$0.88^{+0.11}_{-0.11}$	$7.3^{+5.4}_{-3.0}$	$1.9^{+0.8}_{-0.3}$	$0.51^{+1.1}_{-0.51}$	$0.56^{+\infty}_{-0.55}$	56/62 = 0.92

[a] The notation pcf(ray) indicates a Raymond model with a partial covering absorber.
[b] Hydrogen column density in units of 10^{22} per centimeter squared.
[c] Covering fraction.
[d] Plasma temperature in kiloelectron volts.
[e] Plasma emission normalization equals $8.4 \times 10^{-50}(4\pi d^2)$ times the emission measure.

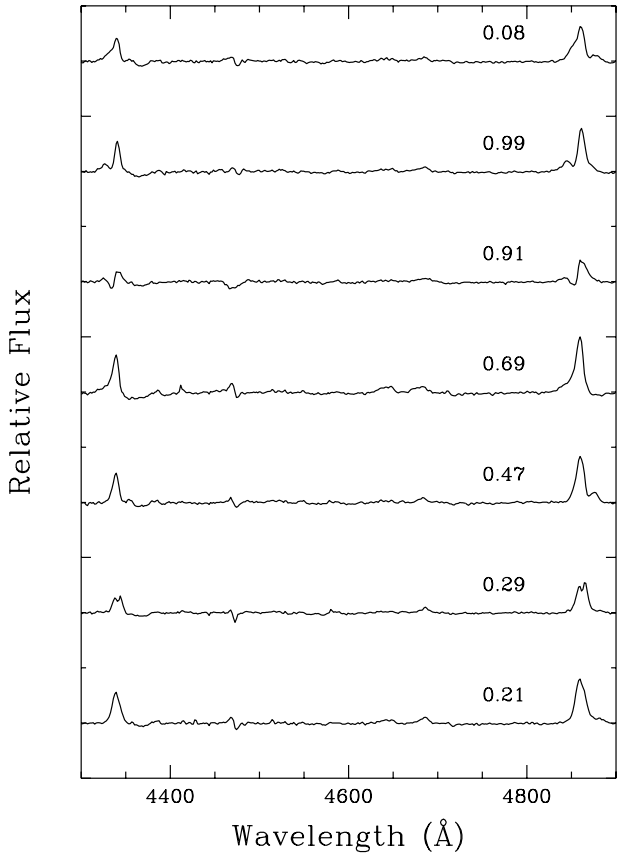


FIG. 3.—Representative blue spectra of LS Peg throughout its orbit. Phases are marked above each spectrum.

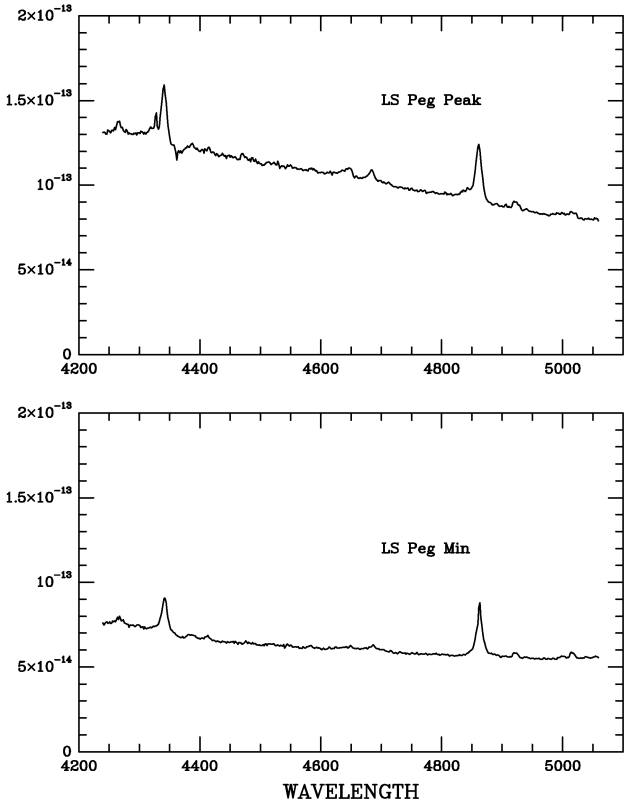


FIG. 4.—Difference between spectra at the low and high points of the V light curve. The top spectrum is at JD 2,451,141.668, and the bottom one is at JD 2,451,141.606 in Fig. 2.

in Figure 2. Unfortunately, the X-ray count rate is too low to try to match up the flickering events.

The optical spectra show the typical behavior of LS Peg, with prominent high-velocity wings and absorption in the Balmer and He I lines (Szkody 1991; TTP; MRC). Using the ephemeris of TTP (which is accurate to 0.08 phase at our epoch), the maximum absorption in He I λ4471 and on the blue side of the Balmer lines occurs at phase 0.7–0.0, and the crossing of the He I absorption from red to blue at phase 0.8, as reported by TTP. Examples of the orbital changes for our blue spectra (which extend the blue coverage from TTP) are shown in Figure 3. We attempted to match up the prominent dips and peaks in the photometry (Fig. 2) with the spectra to see whether the quasi-periodic oscillations (QPOs) were coming from the continuum or line-emitting areas. While the lines go through large changes due to the absorption effects during half the orbit, there is no specific line feature that could be attributed to the low or high points of the light curve. However, it was generally true that the entire continuum decreased during the low times, with the largest decrease occurring at the blue end of the spectrum. Figure 4 shows the faintest spectrum (which occurs on JD 2,451,141.61 in Fig. 2 and at orbital phase 0.40) compared with the brightest (which occurs near time JD 2,451, 141.67 and at phase 0.77). This color dependence of the continuum decrease, together with a lack of change of the QPOs during the phases when the line absorption effects are most prominent, argues that QPOs arise from variations in the inner, hotter portions of the disk.

4. T LEO

The past X-ray data on T Leo consist of *ROSAT* observations showing a relatively high count rate (0.63 counts s^{-1}) with a poor fit to a single bremsstrahlung component and a sparse light curve with variability evident on orbital timescales (Richman 1996). Unlike LS Peg, the count rates obtained with *ASCA* were close to those expected; i.e., 0.290 ± 0.003 counts s^{-1} for SIS 0.6–8 keV and 0.173 ± 0.003 counts s^{-1} for GIS 0.8–8 keV with a 2–6 keV flux of 5.2×10^{-12} ergs s^{-1} cm^{-2}; Table 2. The light curves were extracted in the same manner as for LS Peg and were folded on the orbital period of 0.0588190 (SS84). Since the existing ephemeris was not accurate enough to extrapolate to the current epoch, the absolute phase was determined by fitting a sine function to the velocity curve obtained from the Hα and Hβ lines of the spectra immediately following the *ASCA* observation. With the known orbital period fixed, the γ-velocity and K semiamplitude and phases were determined. The zero of the phase was then set so that it corresponded to the red-to-blue crossing of the γ-velocity (this occurred at 1128 UT on 14 December. The folded *ASCA* light curves are shown in Figure 5. The background throughout the observation was small and stable (0.04–0.07 counts s^{-1}).

All the light curves show an increase in count rate of about 30% between phase 0.8 and 1.0. These light curves consist of 15 cycles with the phase 0.8–1.0 points compiled from five different cycles. While this means that it is not due to a single transient event, the short (20 hr) length of the observation does not allow us to speculate on its long-term stability. This phase interval presents the observer with the most direct view of the stream interaction with the disk and is the same phase at which U Gem exhibits absorption dips. However, here the feature is in emission. In U Gem, the

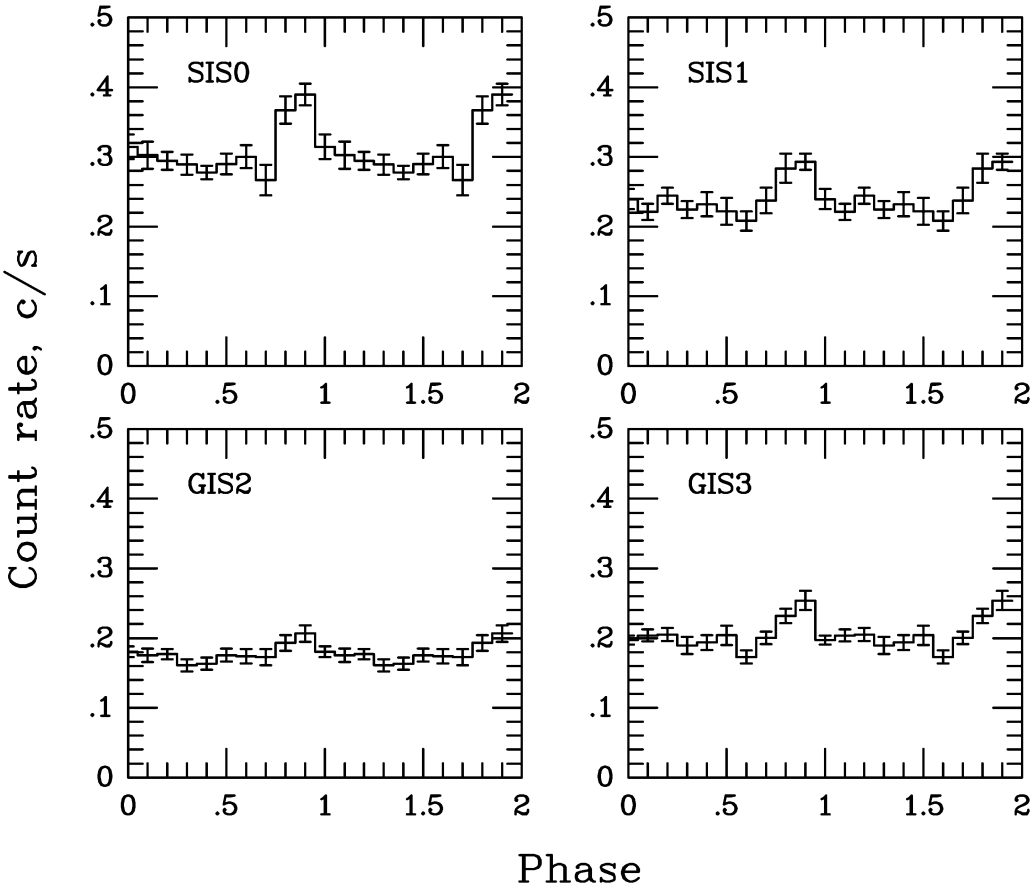


FIG. 5.—*ASCA* light curves of T Leo folded on its orbital period

absorption was energy dependent (visible between only 0.5 and 2 keV), while we could see no change in the amplitude in the light curves of T Leo at energies below and above 2 keV. Since the *ROSAT* data on T Leo compiled by Richman (1996) entail only 5 ks of data and the phasing uncertainty is 0.5 from the SS84 ephemeris, we cannot directly compare our result with the softer *ROSAT* energies.

As for LS Peg, the SIS and GIS spectra were combined, regrouped, and fitted with models using XSPEC. The results of the fits and 90% confidence intervals are summarized in the top of the body of Table 4. The best-fit single temperature ($kT \sim 5$ keV) model with a low column absorber (wabs) gives systematic residuals below 1 keV, while a two-temperature model gives a slightly better statistical fit to the data (Fig. 6). When fitting GIS spectra, the column density was fixed to the best-fit value found from the SIS spectrum; allowing it to vary resulted in unrealistic values.

Spectra during phase 0.8–1.0 ("high" phase seen in the folded light curves) and phase 0.0–0.8 ("low" phase) were

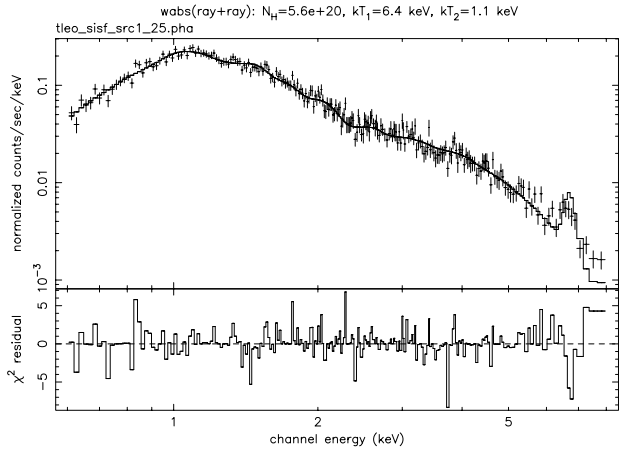


FIG. 6*a*

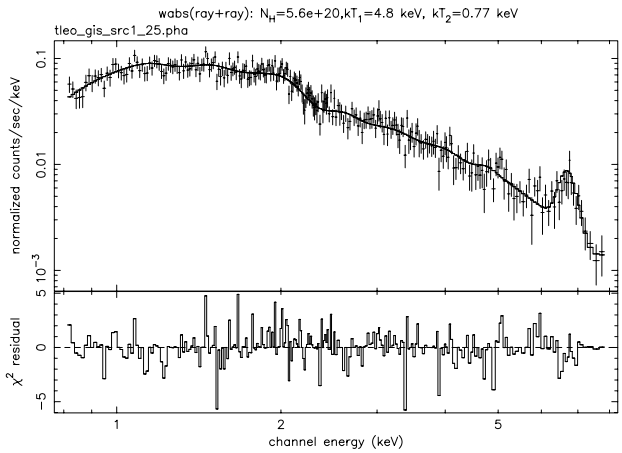


FIG. 6*b*

FIG. 6.—Two-temperature plasma emission model fitted to the combined (*a*) SIS and (*b*) GIS spectra of T Leo

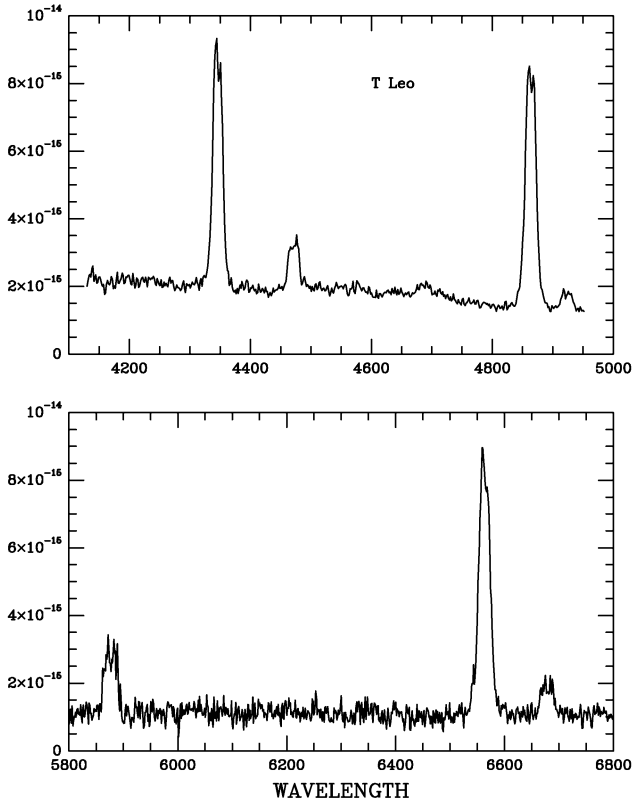


FIG. 7.—Typical blue and red spectrum of T Leo

also fitted with absorbed thermal plasma emission models in order to investigate any differences in the physical conditions of the plasma during these phases. These results are also tabulated in Table 4. Both the high- and low-phase spectra are well represented by the one-temperature model with $kT \sim 5$ keV, and there is no significant difference in the column density nor the plasma temperature during the high and low phases (which is consistent with the lack of amplitude change in the light curve at low vs. high energies). Only the normalization, which is proportional to the emission measure, is higher during the high phase. This behavior is very different than the *ASCA* light curves of U Gem (Szkody et al. 1996), which show increased column during the absorption dips. However, the lower X-ray flux and temperature fit for T Leo are indicative of a lower accretion rate. Under the Armitage & Livio scenario, we would expect more material to flow over the disk and less to be thrown up into the halo at low accretion rates. Thus, the differences between the systems could be due to the difference in mass transfer.

As T Leo shows no orbital variation in U, B, or V continuum light during quiescence (SS84), it is somewhat surprising that there is a phase variation at X-ray wavelengths. An orbital narrow-emission line component in Hα was evident in past data (SS84). It was located at phase 0.14, the opposite side of the disk from a usual hot spot. In order to get further information on the stream flow and determine whether it could be connected to the enhanced emission seen in the X-ray near phase 0.9, we constructed Doppler

TABLE 4

XSPEC MODEL PARAMETERS FOR FITS TO T LEO *ASCA* SPECTRA

		HOT COMPONENT		COOL COMPONENT		
DETECTOR AND MODEL[a]	N_H[b]	kT_1[c]	N_1[d]	kT_2[c]	N_2[d]	χ^2_ν
SIS:						
wabs(ray)	$2.9^{+1.2}_{-1.2}$	$5.1^{+0.3}_{-0.3}$	$7.2^{+0.1}_{-0.1}$			318/236 = 1.3
wabs(ray+ray)	$5.6^{+2.6}_{-1.9}$	$6.3^{+0.7}_{-1.0}$	$6.6^{+0.5}_{-0.2}$	$1.1^{+0.03}_{-0.19}$	$0.53^{+0.16}_{-0.27}$	264/234 = 1.1
GIS:						
wabs(ray)	2.9	$4.3^{+0.2}_{-0.2}$	$7.6^{+0.1}_{-0.1}$			265/260 = 1.0
wabs(ray+ray)	5.6	$4.8^{+0.5}_{-0.4}$	$7.1^{+0.3}_{-0.3}$	$0.77^{+0.18}_{-0.64}$	$0.45^{+0.21}_{-0.16}$	230/258 = 0.89
Phase 0.8–1.0						
SIS:						
wabs(ray)	$4.1^{+3.4}_{-2.8}$	$4.8^{+0.6}_{-0.5}$	$8.4^{+0.4}_{-0.4}$			104/97 = 1.1
wabs(ray+ray)	$3.8^{+3.4}_{-3.1}$	$11^{+30}_{-3.8}$	$6.1^{+1.4}_{-1.9}$	$1.8^{+1.1}_{-0.5}$	$2.3^{+2.4}_{-1.5}$	94/95 = 0.99
GIS:						
wabs(ray)	4.1	$4.5^{+0.6}_{-0.5}$	$8.5^{+0.4}_{-0.4}$			99/75 = 1.3
wabs(ray+ray)	3.8	$5.1^{+0.8}_{-0.6}$	$8.1^{+0.4}_{-0.4}$	$0.10^{+0.65}_{-0.06}$	$305^{+\infty}_{-305}$	81/73 = 1.1
Phase 0.0–0.8						
SIS:						
wabs(ray)	$2.9^{+1.4}_{-1.3}$	$5.1^{+0.3}_{-0.3}$	$6.9^{+0.2}_{-0.2}$			287/212 = 1.4
wabs(ray+ray)	$6.9^{+2.7}_{-2.8}$	$5.7^{+1.3}_{-0.5}$	$6.5^{+0.3}_{-0.4}$	$0.99^{+0.13}_{-0.13}$	$0.39^{+0.28}_{-0.15}$	240/210 = 1.1
GIS:						
wabs(ray)	2.9	$4.2^{+0.2}_{-0.2}$	$7.3^{+0.2}_{-0.2}$			236/236 = 1.0
wabs(ray+ray)	6.9	$4.6^{+1.1}_{-0.4}$	$6.9^{+0.3}_{-0.8}$	$0.84^{+0.28}_{-0.32}$	$0.43^{+0.62}_{-0.18}$	216/234 = 0.92

[a] The notation wabs(ray) indicates a Raymond model with a uniform absorber.
[b] The unit is 10^{20} per square centimeter.
[c] The unit is the kiloelectron volt.
[d] Normalization equals $8.4 \times 10^{-50}(4\pi d^2)$ times the emission measure.

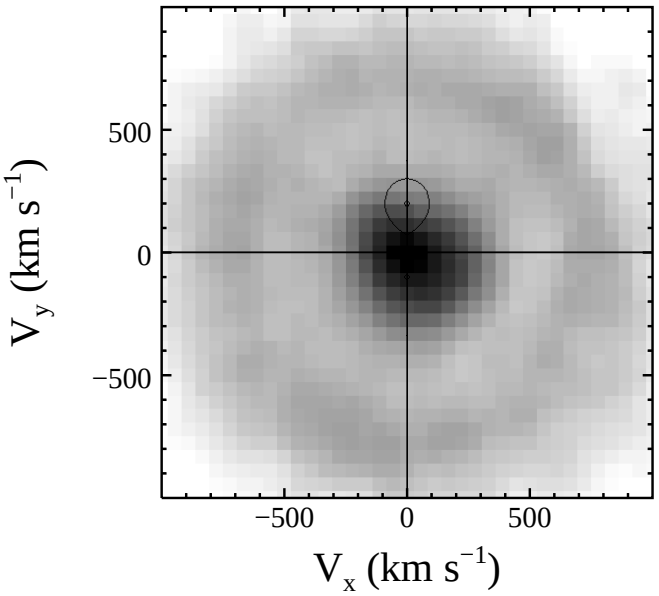


FIG. 8*a*

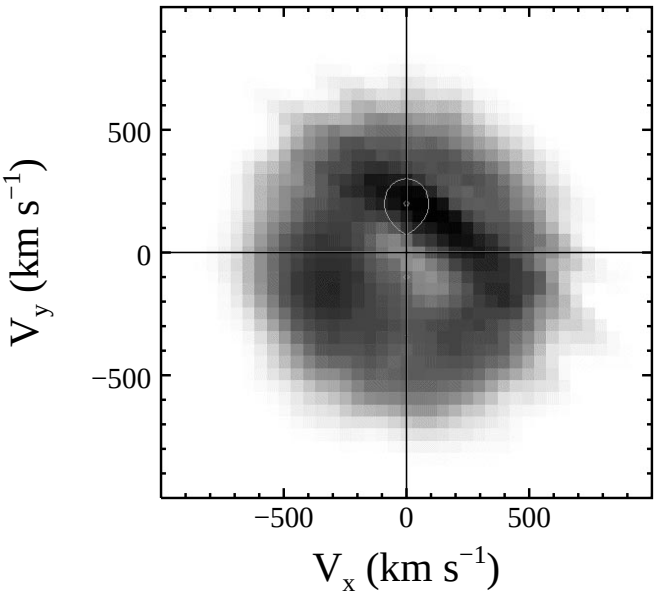


FIG. 8*b*

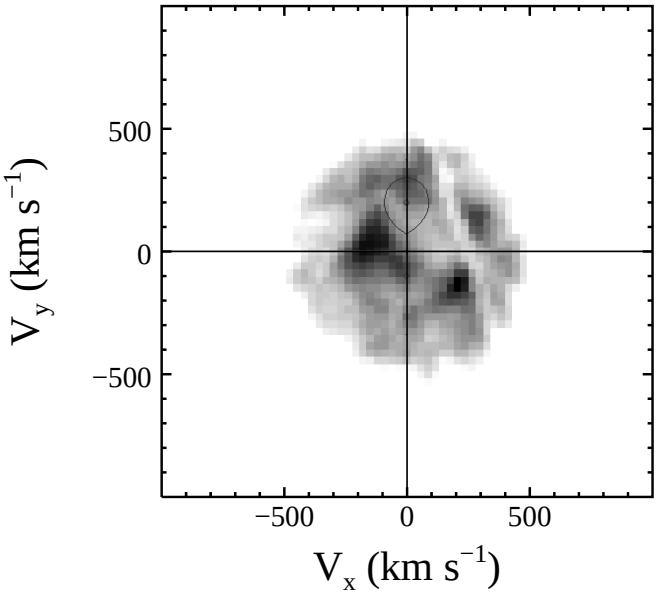


FIG. 8*c*

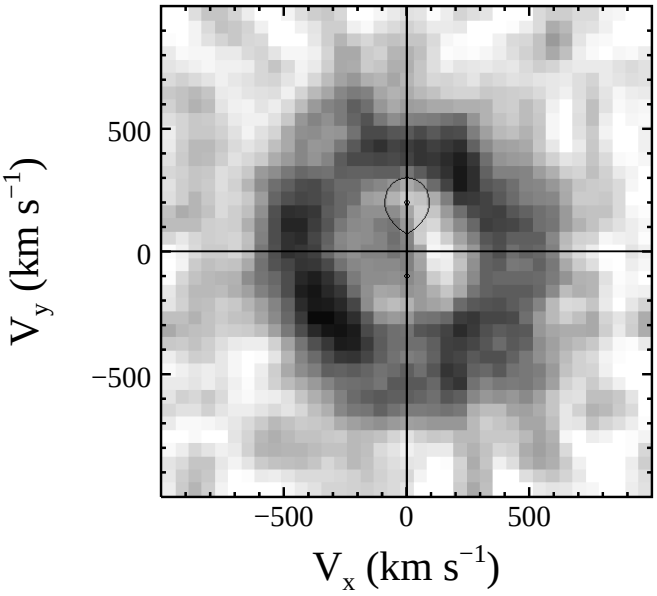


FIG. 8*d*

FIG. 8.—Doppler tomograms of T Leo for (*a*) Hγ, (*b*) Hβ, (*c*) Hα, and (*d*) He I λ 4471

maps from the T Leo optical spectra that were obtained about 13 hours after the *ASCA* observations ended. The tomograms were constructed using a Fourier-filtered back-projection program provided by Keith Horne (Horne 1991) and modified by D. W. Hoard to provide phase-averaging and plotting capabilities. Since T Leo does not eclipse there is no fiducial phasing point, so the red-blue crossing of the emission lines was used to set the zero point (same phasing used for the *ASCA* light curve). Typical spectra are shown in Figure 7 and the tomograms are shown in Figure 8.

These tomograms show a wide range in appearance, from a concentrated region of emission near the center of mass for Hγ, to a location in the disk near phase 0.1 in Hβ, to several emission zones (near phases 0.2, 0.3, and 0.8) in Hα. In addition, the tomogram of He I λ4471 is a ring. There are some artifacts (evident as diagonal streaks in the Hβ and Hα tomograms), likely due to two gaps in the data caused by equipment problems during the night. While all phases were covered during the 3 hour interval of observation and most phases were observed twice, resulting in an average phase resolution of 0.01–0.05 phase, the phase intervals 0.27–0.51 and 0.72–0.87 have lower (0.08) phase resolution. However, this cannot account for the large differences evident between the low- and high-velocity regions, especially for the Hβ, Hγ, and He I lines, which were all obtained with the same spectrograph with the same phase coverage. The concentrated emission seen at $+V_x = 300$ and $+V_y = 150$ in the Hα tomogram may be related to the narrow component previously seen in Hα (SS84), while the more extended emission rising from the $-V_x$ line to $+V_y$ values is likely the stream flow (see typical systems in Kaitchuck et al. 1994). If this is the case, the emission from the stream is stronger

than that from the opposite side of the disk, contrary to the data obtained in 1982, and the increased X-ray emission may be related to more emitting plasma along that line of sight. However, the lack of good phase resolution between phase 0.25 and 0.35 makes it difficult to determine accurately the emission structure on the far side of the disk, e.g., the spot where $+V_x = 300$ and $+V_y = 150$ may be connected to the structure seen where $+V_x = 200$ and $-V_y = 150$.

5. CONCLUSIONS

Our *ASCA* observations of LS Peg have revealed the faint, hard X-ray spectrum that is typical of high mass transfer rate CVs. It is likely that the previous higher X-ray flux and harder spectrum measured with *Ginga* was due to the presence of an additional source in the field of view. The *ASCA* data are fitted with a 6–7 keV thermal plasma model that is partially absorbed with a high column ($\log N_{\rm H} = 22.7$). These parameters are typical of magnetic accretors or could be caused by a halo of material thrown up by the stream impact in this high accretion rate system. The simultaneous optical photometry shows the 19 minute QPOs that are typical for LS Peg, and the spectra exhibit the usual absorption and high-velocity components that have previously characterized this SW Sex star. A comparison of the spectra at the brightest and faintest times of the QPO implies an association of the QPO variability with the hotter inner disk areas.

The *ASCA* light curve of T Leo shows enhanced flux during phases 0.8–1.0. Unlike U Gem, which shows a decrease in flux near these phases, this enhancement is not associated with a change in temperature nor column, but appears to be an increase in emission measure. The entire spectrum is consistent with a 4–6 keV thermal spectrum with column of $3–5 \times 10^{20}$ cm^{-2}, with a small contribution from a cooler 1 keV component. Doppler tomograms constructed from optical spectra obtained within a few hours of the *ASCA* observations show a variety of emission sites for different Balmer and He I lines. There is evidence for some emission from the stream, as well as an impact site on the far side of the disk. The lower accretion rate of this system compared with U Gem may account for the differences in their X-ray spectra and light curves.

P. S. and K. N. acknowledge partial support from NASA ADP grant NAG 5-8374 and LTSA grant NAG 5-3345. We are grateful to Keith Horne and D. W. Hoard for making their software for Doppler tomography available to us.

REFERENCES

Armitage, P. J., & Livio, M. 1996, ApJ, 470, 1024
———. 1998, ApJ, 493, 898
Casares, J., Martinez-Pais, I. G., Marsh, T. R., Charles, P., & Lazaro, C. 1996, MNRAS, 278, 219
Frank, J., King, A. R., & Lasota, J. P. 1987, A&A, 178, 137
Garnavich, P., & Szkody, P. 1992, J. AAVSO, 21, 81
Hirose, M., Osaki, Y., & Mineshige, S. 1991, PASJ, 43, 809
Hoard, D. W., Thorstensen, J. R., & Szkody, P. 2000, ApJ, 537, 936
Horne, K. 1991, in Fundamental Properties of Cataclysmic Variable Stars, ed. A. Shafter (San Diego: San Diego State Univ.), 23
Ishida, M., Fujimoto, R., & Matsuzaki, K. 1996, in Cataclysmic Variables and Related Objects, ed. A. Evans & J. H. Wood (Dordrecht: Kluwer), 259
Kaitchuck, R. H., Schlegel, E. M., Honeycutt, R. K., Horne, K., Marsh, T. R., White, J. C., II, & Mansperger, C. S. 1994, ApJS, 93, 519
Long, K. S., Mauche, C. W., Raymond, J. C., Szkody, P., & Mattei, J. A. 1996, ApJ, 469, 841
Martinez-Pais, I. G., Rodriguez-Gil, P., & Casares, J. 1999, MNRAS, 305, 661 (MRC)
Mason, K. O., Cordova, F. A., Watson, F. G., & King, A. R. 1988, MNRAS, 232, 779
Richman, H. 1996, ApJ, 462, 404
Rodriguez-Gil, P., Casares, J., Martinez-Pais, I., Hakala, P., & Steeghs, D. 2001, ApJ, 548, L49
Shafter, A. W., & Szkody, P. 1984, ApJ, 276, 305 (SS84)
Szkody, P. 1991, in Fundamental Properties of Cataclysmic Variable Stars, ed. A. Shafter (San Diego: San Diego State Univ.), 56
Szkody, P., Garnavich, P., Castelaz, M., & Makino, F. 1994, PASP, 106, 616
Szkody, P., Garnavich, P., Holberg, J., Silber, A., & Pastwick, L. 1997, AJ, 113, 2276
Szkody, P., Long, K. S., Sion, E. M., & Raymond, J. C. 1996, ApJ, 469, 834
Tanaka, Y., Inoue, H., & Holt, S. S. 1994, PASJ, 46, L37
Taylor, C. J., Thorstensen, J. R., & Patterson, J. 1999, PASP, 111, 184 (TTP)
Verbunt, F., Bunk, W. H., Ritter, H., & Pfeffermann, E. 1997, A&A, 327, 602
Warner, B. 1995, Cataclysmic Variable Stars (Cambridge: Cambridge Univ. Press)
Watson, M. 1995, in ASP Conf. Ser. 85, Cape Workshop on Magnetic Cataclysmic Variables, ed. D. H. Buckley & B. Warner (San Francisco: ASP), 259